A continuous-wave optical parametric oscillator around 5-μm wavelength for high-resolution spectroscopy

J. Krieg,[a] A. Klemann, I. Gottbehüt, S. Thorwirth, T. F. Giesen, and S. Schlemmer
I. Physikalisches Institut, Universität Köln, Zülpicher Str. 77, 50937 Köln, Germany

(Received 24 February 2011; accepted 11 May 2011; published online 16 June 2011)

We present a continuous-wave optical parametric oscillator (OPO) capable of high resolution spectroscopy at wavelengths between 4.8 μm and 5.4 μm. It is based on periodically poled lithium niobate (PPLN) and is singly resonant for the signal radiation around 1.35 μm. Because of the strong absorption of PPLN at wavelengths longer than 4.5 μm, the OPO threshold rises to the scale of several watts, while it produces idler powers of more than 1 mW and offers continuous tuning over 15 GHz. A supersonic jet spectrometer is used in combination with the OPO to perform measurements of the transient linear molecule Si_2C_3 at 1968.2 cm^{-1}. Fifty rovibrational transition frequencies of the ν_3 antisymmetric stretching mode have been determined with an accuracy on the order of 10^{-4} cm^{-1}, and molecular parameters for the ground and the $v_3 = 1$ state have been determined most precisely. © *2011 American Institute of Physics*. [doi:10.1063/1.3596569]

I. INTRODUCTION

A versatile radiation source for spectroscopic measurements ideally provides broadband frequency coverage and sufficient power while maintaining high spectral resolution. In the mid-infrared (MIR) region, suitable radiation sources are rare. For many years, lead-salt diode lasers have been used in high-resolution spectroscopy.[1] These devices can be manufactured to emit at any desired frequency in the MIR; however, they offer only limited tunability of a few wavenumbers. Other drawbacks are poor spectral quality due to multi-mode emission, low optical power of often less than 1 mW, and astigmatic beam profiles. Being superior to lead-salt diode lasers in all the above respects, quantum-cascade lasers have emerged as alternative MIR radiation sources over the last years and have demonstrated their potential in many high-resolution spectroscopic experiments.[2,3]

Even greater frequency bandwidth can be achieved employing nonlinear frequency mixing. In the region towards the near infrared between 1 μm and 4 μm wavelength, optical parametric oscillators (OPOs) have become important, especially because the necessary phase matching in the nonlinear material can easily be achieved via periodic poling of the nonlinear material (quasi phase-matching (QPM (Ref. 4))), which has been used successfully in OPOs since the mid 1990s.[5] QPM materials, such as periodically poled lithium niobate (PPLN) have been commercially available for a number of years now, turning continuous-wave (cw) OPOs into high-bandwidth, high-power devices applicable for high-resolution spectroscopy.[6–8]

Up to this point, the frequency coverage of OPOs usually excluded the wavelength region longward of 4.7 μm due to the rapidly increasing attenuation coefficient of PPLN ($\alpha \approx 1$ cm^{-1} at 5 μm wavelength[9]). Only two cw OPOs, both based on PPLN, have so far been demonstrated[10,11] at 5 μm, both of which were suffering, however, from serious limitations in the continuous tuning range. For high-resolution experiments, this property is of utmost importance.

At present, no periodically poled nonlinear material other than PPLN is available commercially for the MIR region. However, if output power on a mW-scale is sufficient for the experiment, one just needs to overcome the oscillation threshold which is on the order of several watts (Ref. 11) for singly resonant systems and therefore provided by common pump lasers.

In the present investigation, we introduce a cw PPLN OPO working around 5 μm with a 250 cm^{-1} bandwidth, which is to our knowledge the first OPO in this regime suitable for high-resolution spectroscopy. The OPO has been integrated in a spectrometer featuring a laser ablation unit for the production of transient species in the gas phase and a sensitive detection scheme. High spectral resolution and high sensitivity allow for the observation of weakly absorbing species and short-lived molecular radicals in a supersonic jet. The performance of the system has been tested through a study of the fundamental vibration mode ν_3 of the linear molecule Si_2C_3, for which an improved set of molecular parameters is presented.

II. CONTINUOUS-WAVE 5-μm OPO

A. Experimental setup

The OPO has a standard setup as seen in other cw OPO systems with a four mirror ring-cavity, in which only the near infrared signal radiation is kept resonant (singly resonant OPO), as first described in Ref. 12. This configuration is quite standard for these systems until today.[13] The setup of the OPO can be seen schematically in Fig. 1. A continuous-wave pump laser at a wavelength of $\lambda = 1.064$ μm (Innolight Mephisto MOPA series[14]) is driving the OPO. Its maximum output power is 10 W, and the linewidth is less than 5 kHz over a period of 100 ms, and frequency drifts are less than 1 MHz/min. A half-wave plate in combination with a

[a]Electronic mail: krieg@ph1.uni-koeln.de.

 © 2011 American Institute of Physics

Downloaded 10 Mar 2012 to 134.95.83.67. Redistribution subject to AIP license or copyright; see http://rsi.aip.org/about/rights_and_permissions

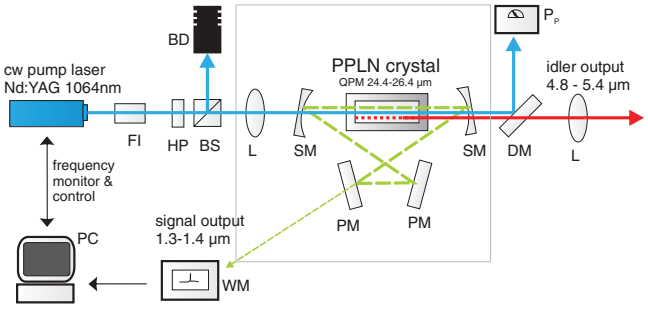

FIG. 1. (Color online) Schematic setup of the OPO. Denominations are as follows: FI – Faraday isolator; HP – half-wave plate; BS – polarizing beam splitter; BD – beam dump; L – spherical lens; SM – concave mirror; PM – plane mirror; DM – dichroic mirror; WM – wavemeter; P_P – power meter for pump.

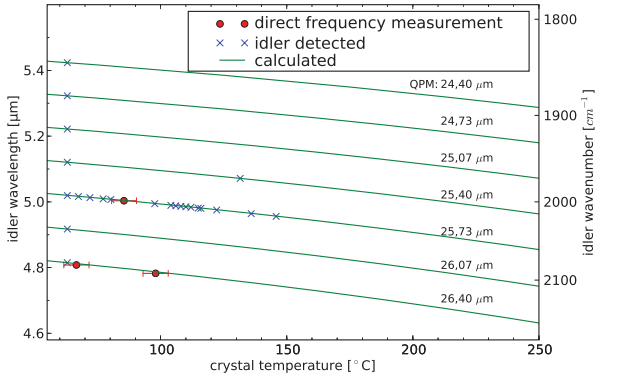

FIG. 2. (Color online) Frequency coverage of the OPO system. Crosses designate measurements of temperatures of the crystal for which idler radiation was detected. Points with error bars designate frequencies directly measured with a wavemeter.

polarizing beam splitter allows the variation of pump power for the OPO while the pump laser is working at constant parameters to maintain stable operating conditions. The pump beam has a focus in a crystal of 5% vol. MgO-doped $LiNbO_3$ is acquired from HCP photonics, Taiwan, which is periodically poled to achieve phase matching. The PPLN crystal features seven poling periods equally distributed over the interval from 24.4 μm to 26.4 μm. These poling periods translate into an accessible wavenumber range from 1850 cm^{-1} to 2150 cm^{-1}. The crystal is anti-reflection (AR) coated for the relevant waves in the mixing process (<1% for signal and pump and <5% for idler). The home-built oven harboring the crystal is temperature-controlled with an analog stabilization scheme in a range between 50 and 200 °C to vary the output frequencies within the same poling period.

Optical feedback in the signal regime is achieved via a bow-tie ring resonator consisting of high-reflectivity mirrors (>99.99% for signal, AR for pump and idler) purchased from Layertec.[15] Two mirrors are plane and two are plane-concave with a radius of curvature of 100 mm. A simulation for the beam propagation in the cavity using Gaussian optics results in a beam waist of 100 μm. As proposed by Vainio *et al.*, no intracavity frequency selecting elements are used.[8]

Coarse selection of the idler frequency is performed via the crystal grating period and temperature. Continuous idler tuning is then realized by tuning the pump laser with a signal frequency fixed by the signal cavity. This permits a scanning range of >80 GHz, of which windows of >15 GHz are mode-hop free, being limited by the pump laser.

B. OPO performance

With the new OPO, radiation can be generated over a broad frequency range in the wavenumber interval from 1850 cm^{-1} to 2150 cm^{-1}. This is a substantial extension of the wavelength range of a PPLN-based OPO. Therefore, it is interesting to compare the performance of our OPO to the expectations derived from simple model calculations, which will be discussed in more detail below. Figure 2 shows the bandwidth of the system. Theoretical wavelength curves for the different poling periods used in the crystal are also plotted. Each curve fulfills the phase matching expression $\Delta k = 0$,

$$\Delta k = \frac{2\pi n_p \nu_p}{c} - \frac{2\pi n_s \nu_s}{c} - \frac{2\pi n_i \nu_i}{c} - \frac{2\pi}{\Lambda} = 0, \qquad (1)$$

for collinear interaction of the waves, with n being the refractive index and ν being the frequency of the wave, and indices (p, s, i) from now on consistently represent the pump, signal, and idler wave, respectively. Λ is the poling period of the PPLN material. The Sellmeier equation for $LiNbO_3$ with coefficients taken from Ref. 17 gives all information needed to calculate the temperature dependent indices of refraction. For experimental determination of the frequency coverage, the idler frequency was measured directly using a wavemeter (Bristol Instruments, model 621A-IR). However, the idler power is barely sufficient to meet the minimum input power required by the wavemeter; therefore, only three exemplary wavelengths were chosen for comparison (red dots in Fig. 2). Typical OPO output powers vary a lot and are typically in the range between 1 to 10 mW at pump powers between 6 W and 8 W. Crosses in Fig. 2 designate regions, where idler power was detected without a direct frequency measurement using the wavemeter.

To compare our results with a simple model, the coupled wave equations for the field amplitudes $\mathcal{E}_l$ $(l = p,s,i)$ of the relevant waves (see, for example, Ref. 18) need to be corrected for absorption in the crystal:

$$\frac{\partial}{\partial z}\mathcal{E}_p(z) = i\gamma_p\,\mathcal{E}_s(z)\mathcal{E}_i(z)\,e^{-i\Delta kz} - \frac{\alpha_p}{2}\mathcal{E}_p(z), \qquad (2)$$

$$\frac{\partial}{\partial z}\mathcal{E}_s(z) = i\gamma_s\,\mathcal{E}_p(z)\mathcal{E}_i^*(z)\,e^{+i\Delta kz} - \frac{\alpha_s}{2}\mathcal{E}_s(z), \qquad (3)$$

$$\frac{\partial}{\partial z}\mathcal{E}_i(z) = i\gamma_i\,\mathcal{E}_p(z)\mathcal{E}_s^*(z)\,e^{+i\Delta kz} - \frac{\alpha_i}{2}\mathcal{E}_i(z). \qquad (4)$$

Here, $\gamma_l = (2\pi\nu_l d)/(n_l c)$ $(l = p,s,i)$ is the nonlinear coupling factor, where d is the nonlinear material coefficient, and the factors α_l are the absorption coefficients of the nonlinear material for the corresponding frequency resulting from the Lambert–Beer law for the intensity of a wave $I_l(z) = I_l(0)e^{-\alpha_l z}$. I_l can be written as $I_l = c\varepsilon_0 n_l|\mathcal{E}_l|^2/2$.

Downloaded 10 Mar 2012 to 134.95.83.67. Redistribution subject to AIP license or copyright; see http://rsi.aip.org/about/rights_and_permissions

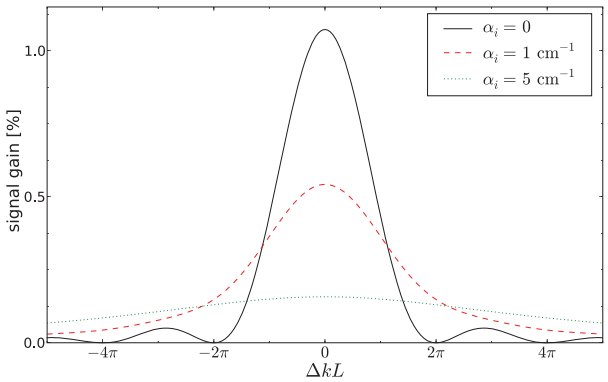

FIG. 3. (Color online) Calculated signal gain curves at a pump power of 1 W in the limit of plane waves for different idler absorption coefficients α_i. Pump wavelength is 1064 nm and idler wavelength is 5 μm, the beam radius is set to 100 μm, crystal length is 5 cm. At this idler wavelength, α_i is realistically $\approx 1\ \mathrm{cm}^{-1}$ (see Ref. 9).

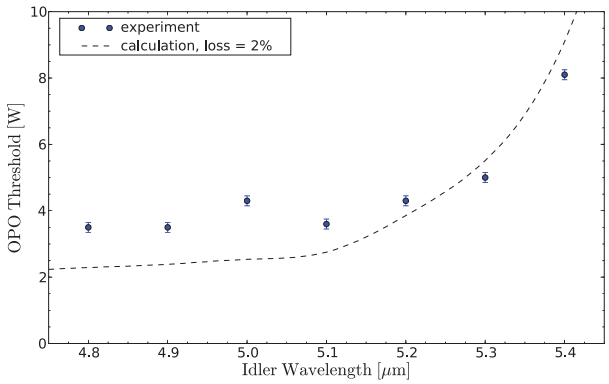

FIG. 4. (Color online) Threshold of the home-built OPO system in the mid-infrared around 5 μm wavelength. The theoretical curve is based on a calculation featuring the solution of the coupled wave equations (2)–(4) with idler absorption in the limit of plane waves. Data for the absorption coefficient is taken from Myers *et al.* (see Ref. 9) For details see text.

Equations (3) and (4) have been solved analytically in the limit of a non-depleted pump intensity (which means that $(\partial/\partial z)\mathcal{E}_p(z) = 0$ and Eq. (2) vanishes) and plane waves, which is summarized in Appendix B. Lowenthal had a similar approach in solving the coupled wave equations with idler absorption, where the effects of Gaussian beams were included in a heuristic fashion.[19] Figure 3 shows the calculated gain for the signal wave with a 1064 nm pump wave of 1 W power producing an idler wave of 5 μm wavelength. The signal gain curve is plotted for three different idler attenuation coefficients to show the influence of idler absorption. Beam radii are 100 μm, crystal length is 5 cm, and the PPLN nonlinear coefficient is $d = 17\mathrm{pm/V}$. The gain profile becomes smaller with increasing idler absorption, which raises the oscillation threshold. Since the signal amplitude increase from Eq. (3) also depends on the idler amplitude, this behavior is not a surprise. However, the bandwidth of the parametric process also increases quite drastically with idler absorption which can be desirable, depending on the application. In our experiment, larger bandwidths increase the possibility of mode-hops and are therefore another drawback of the larger absorption.

The threshold pump power P_{th} is calculated by setting the signal gain equal to $V/(1-V)$, where V is the cavity round trip loss of the signal intensity. Without idler absorption, one obtains with perfect phase matching $\Delta k = 0$ (see Appendix B, or Ref. 18):

$$P_{\mathrm{th}} = \frac{c\varepsilon_0 n_p n_s n_i \lambda_s \lambda_i}{8\pi^2} \frac{A}{d^2 L^2} \frac{V}{1-V}, \tag{5}$$

where L is the crystal length, c is the speed of light, A is the beam area, and V are the losses in the signal cavity. Including idler absorption in the solution of the coupled wave equations results in a wavelength dependent threshold because of the varying idler absorption coefficient. Figure 4 shows the measured threshold as well as the calculation for a cavity with a signal loss per cavity round trip of $V = 2\%$. The idler absorption coefficient is taken from Ref. 9. A near quantitative agreement can be seen. However, the model overestimates the threshold in the longer wavelength part and underestimates it at shorter wavelengths. We attribute this to the absorption of the resonant signal wave due to water vapor in laboratory air, which is more prominent for shorter idler wavelengths. A simulation of this absorption using the HITRAN04 database[16] is shown in Fig. 5. Every transition in the database has been convolved with a Lorentzian profile with a width resulting from its air broadening coefficient (in the range from 10^{-2} to 10^{-3} $\mathrm{cm}^{-1}\ \mathrm{atm}^{-1}$). The simulation is based on the standard atmospheric pressure and a relative humidity of 40%. The absorption graph shows many single lines which overlap and result in a non-negligible background absorption at frequencies next to the transition frequencies of water. At lower signal frequencies, the minimum absorption loss per cavity round trip rises to a level of 10^{-3} and higher. Therefore, water absorption contributes significantly to the loss per cavity round trip and is even the dominating loss process for lower signal frequencies (higher idler frequencies). The contribution of the mirrors to the cavity round trip loss is below 10^{-3}. According to

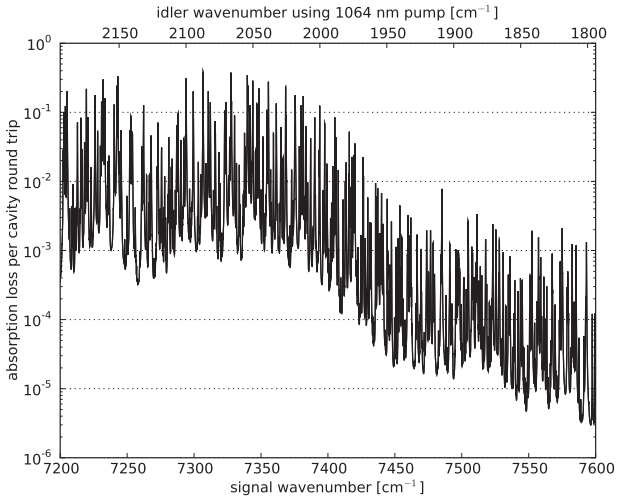

FIG. 5. Cavity round-trip-loss of signal radiation due to absorption of water vapor in laboratory air (~40% relative humidity at room temperature), simulated using the HITRAN04 database.[16] The upper frequency scale gives the corresponding idler wavenumber with an OPO pump wavelength of 1064 nm. For details see text.

Downloaded 10 Mar 2012 to 134.95.83.67. Redistribution subject to AIP license or copyright; see http://rsi.aip.org/about/rights_and_permissions

Eq. (5), the OPO threshold is approximately linear in the loss per cavity round trip, which still holds when including idler absorption. The signal absorption by water then adds to V in Eq. (5), introducing a strong wavelength dependence. Strong variations of the threshold over a range of a few cm^{-1} and the overall increase of the threshold towards shorter idler wavelengths are attributed to this signal absorption. In some small regions of the spectrum accessible to the OPO crystal poling periods, no oscillation at all could be achieved with our 10 W pump laser. However, in most cases it is possible to tune the pump laser to enable oscillation close to the water lines.

On small timescales of less than a millisecond, the linewidth of the OPO was estimated using a high-finesse optical cavity (ZnSe substrate mirrors coated by Lohnstar Optics, Inc.[20]). The idler was scanned fast by piezo-tuning over a resonance peak of the cavity. A sharp fringe of less than 300 kHz full width at half maximum was measured as depicted in Fig. 6. A frequency precision of $\Delta\nu/\nu \approx 5 \times 10^{-9}$ holds for a period of roughly 10^{-4} s.

On larger timescales of seconds, the idler frequency varied in frequency intervals of roughly 10^{-3} cm^{-1}. Given that the frequency precision of the pump is orders of magnitude higher, these variations have to be caused by a signal frequency variation $\Delta\nu_s$, which is defined by the optical path length of the resonator. The following expression holds approximately with the refractive index n_s at the signal frequency ν_s, the optical path length of the resonator L, and the length of the crystal l: $\Delta\nu_s/\nu_s = \Delta L/L \approx l\Delta n_s/L$. Here, the thermal expansion of geometric cavity and crystal lengths can be neglected. With Sellmeier coefficients for $n_s(T)$ taken from Ref. 17, a temperature variation of 1 mK results in a frequency variation $\Delta\nu_s/\nu_s$ of roughly 5×10^{-8}, which translates into a signal and idler uncertainty of 5×10^{-4} cm^{-1} over the time the temperature changes. From this the temperature stability of the oven can be estimated to be better than 10 mK. These slow frequency drifts can be compensated in the experiment with a proper calibration of the scans using a temperature-stable reference interferometer.

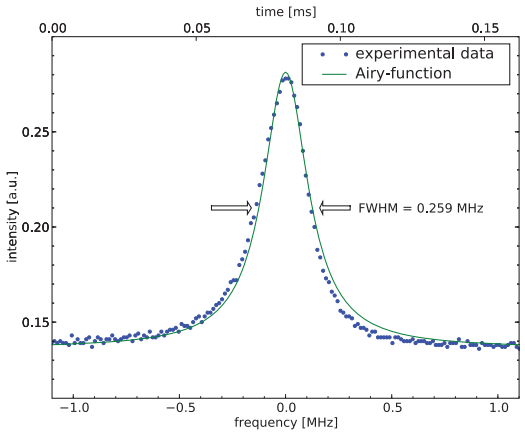

FIG. 6. (Color online) Fringe of a high finesse cavity, measured with a rapid scan of the OPO at 2079 cm^{-1}. The time of the scan elapsed is shown on the upper axis.

III. SPECTROMETER FOR TRANSIENT MOLECULES

Cumulenic structures, such as those present in pure carbon chains C_n, $n = 3, 4, 5\ldots$, exhibit prominent spectroscopic features in the 5-μm wavelength regime.[21] In a first spectroscopic application, we combined the OPO with a sensitive spectrometer to observe stretching vibrations of silicon-carbon clusters, which also exhibit cumulenic bonding. Because these species are short-lived, an effective production mechanism is necessary as well as a sensitive detection scheme. Both are described in the following.

A. Production of species

Carbon-silicon clusters were produced using laser ablation followed by supersonic jet expansion similar to the approach described earlier.[1,2] The experimental setup is drawn schematically in Fig. 7. Radiation of a Q-switched Nd:YAG laser (Continuum Lasers, model INLITE III-30) with a repetition rate of 25 Hz is frequency multiplied and its third harmonic at 355 nm wavelength is then focused onto the solid target rod, which is made of silicon carbide. At helium backing pressures of ≈15 bar, the ablated material is guided through a 7 mm long reaction channel, prior to expansion into a vacuum chamber. As a result of adiabatic cooling, rotational temperatures of ∼20 K are typically found in the jet.

B. Data acquisition

The supersonic jet is oriented perpendicularly to the optical axis of a Herriott-type multipass cell. Up to 66 passes of the OPO idler wave through the jet have been realized, before the idler intensity is detected on an InSb infrared detector (Det. C in Fig. 7).

The jet absorption signal is digitized using an Universal Serial Bus (USB) oscilloscope (PicoScope 4000series, Pico technology, UK). Triggered by the ablation laser, the oscilloscope records typically 50 μs with a sampling rate of ≥ 10 MS/s to a hard disk. Due to the different time of flights of

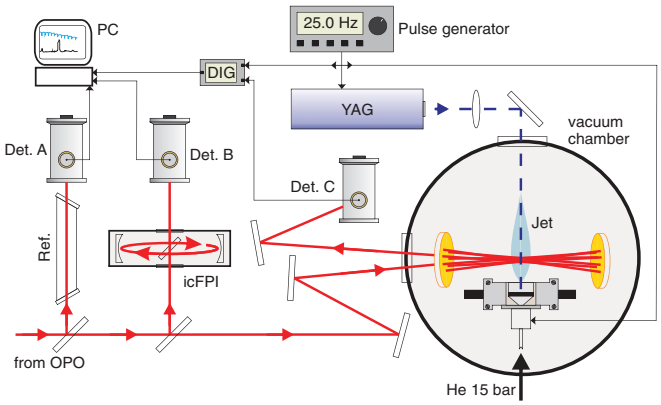

FIG. 7. (Color online) Schematic setup of the jet spectrometer. Parts of the OPO beam are guided through a reference gas cell (Ref.) and a reference interferometer (icFPI) for calibration purposes. The beam passing the jet through a multipass reflection cell is detected and its signal is digitized using an USB oscilloscope (DIG). The jet is produced by ablating solid samples with a high-energy laser and a flow of helium at a high pressure.

Downloaded 10 Mar 2012 to 134.95.83.67. Redistribution subject to AIP license or copyright; see http://rsi.aip.org/about/rights_and_permissions

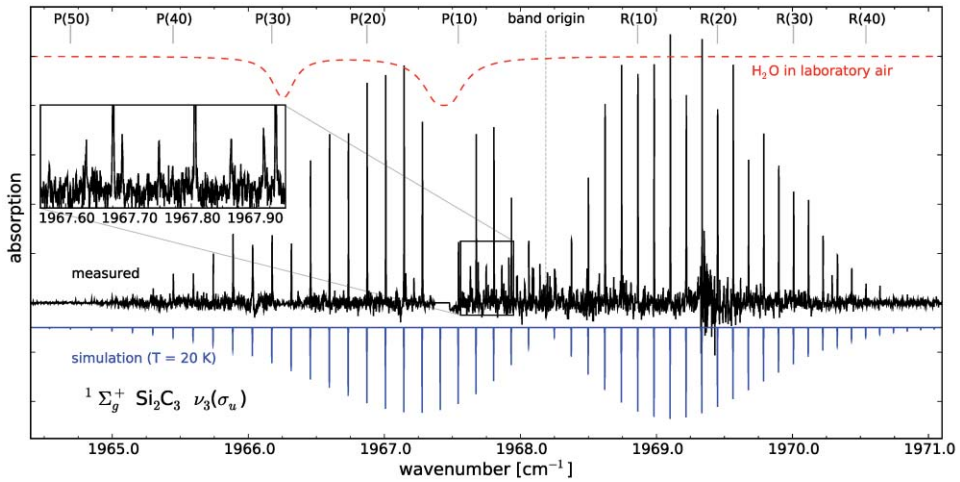

FIG. 8. (Color online) Spectrum of the ν_3 stretching vibration of Si_2C_3. Lines have a spacing of four times the rotational constant, because transitions with odd numbered values of the ground state rotational quantum number J'' are missing due to spin statistics. Transmission of infrared radiation through laboratory air is sketched in the dashed line using a HITRAN simulation. The inset shows a second rotational band, which is probably originating from a hotband involving a vibrational bending mode.

different clusters, the absorption signals of different species produced in the jet expansion can be separated in time. A major advantage over boxcar integrators commonly used in these experiments is the possibility of post-processing of data since the entire time-resolved detector signal is recorded, i.e., the boxcar integrators are software-emulated and the boxcar gates can be optimized after the measurement. This is why different species simultaneously present in the jet can be analyzed using data from a single frequency scan.

In a first rough frequency determination during scans, a wavemeter is used. Because of its limited sensitivity at longer wavelengths (device specified for the wavelength range 1.5 μm to 5.0 μm), a direct measurement of the idler frequency with a beam splitter which feeds part of the idler radiation into the instrument is not possible. However, the idler frequency can be measured indirectly by determination of the signal frequency ν_s using the wavemeter and recording the temperature of the pump laser. With a look-up table which links the temperature of the scanning pump laser with its frequency ν_p, the idler frequency ν_i is simply derived by taking the difference of these two: $\nu_i = \nu_p - \nu_s$. With this method, a frequency accuracy of ~100 MHz is achieved, which is limited by the resolution of the wavemeter. This information greatly supports the assignment of reference gas transitions. Scans are finally calibrated using the simultaneously recorded spectra of a reference gas (using Det. A in Fig. 7) and a reference Fabry-Pérot interferometer (using Det. B in Fig. 7). Details about the frequency calibration of the scans and the hardware used can be found in Appendix A.

IV. FIRST SPECTROSCOPIC RESULT: Si_2C_3

In first experiments carried out with our new OPO spectrometer, we selected linear Si_2C_3 (Si=C=C=C=Si) as a target molecule which belongs to one of the very few silicon-carbon clusters previously studied at high spectral resolution in the gas phase. The molecule has a $^1\Sigma_g^+$ electronic ground state, is centrosymmetric, and features seven vibrational modes (including three doubly degenerate bending modes), the strongest of which is the antisymmetric C–C stretching mode ν_3 located at 1968.2 cm^{-1} (Ref. 22).

In the present study, this band has been reinvestigated by recording a total of 74 individual scans in the frequency interval between 1964 and 1972 cm^{-1}. Each scan was performed by varying the frequency in small steps of around 5 MHz, after having recorded 15 shots of the jet signal, while a single scan of 15 GHz lasts for 30 min at a repetition rate of 25 Hz. Selected regions have been measured more than once to increase the signal-to-noise ratio. Each of the scans was calibrated as described in Appendix A using the interferometer and allene ($H_2C=C=CH_2$) as a reference gas. After that, an averaging algorithm has been applied to the partly overlapping spectra. This algorithm divides the relevant frequency range in bins with a width of 5×10^{-4} cm^{-1} and averages all data in one bin to one single data point. Because of varying jet conditions and idler power transmitted through the multipass cell, line intensities are only correct within ~30% of the line intensity of a single scan, which is why the spectra are normalized in intensity and weighted with their individual noise level beforehand. The resulting spectrum of Si_2C_3 obtained here is shown in Fig. 8. The simulation also shown there has been performed using the program PGOPHER.[23]

In total, 50 transitions from the ν_3 fundamental band in the wavenumber range between 1964.6 cm^{-1} and 1971.1 cm^{-1} were measured, covering rotational transitions P(50) to R(50). Only the P(12) transition could not be measured due to interference with a strong atmospheric water line (Table I). Molecular parameters based on a least-squares fit to a standard linear molecule model using the SPFIT program[24] are shown in Table II. Values by van Orden *et al.* are also shown for comparison as well as *ab initio* values by Botschwina[25] obtained at the coupled-cluster level of theory. The precision in the rotational constants B was enhanced by a factor of five. For this fit, the experimental uncertainty of the frequency positions was conservatively set to 5×10^{-4} cm^{-1}, that results in a rms value of 0.54. Both B values are smaller

Downloaded 10 Mar 2012 to 134.95.83.67. Redistribution subject to AIP license or copyright; see http://rsi.aip.org/about/rights_and_permissions

TABLE I. Measured transition frequencies of the ν_3 antisymmetric stretching band of Si_2C_3 in cm^{-1}. Best fit residuals are also given (see Table II).

J	R(J)	Obs.-calc. ($\times 10^{-3}$)	P(J)	Obs.-calc. ($\times 10^{-3}$)
0	1968.2521	0.59	...	...
2	1968.3762	–0.21	1968.0621	0.00
4	1968.5002	–0.01	1967.9346	0.14
6	1968.6229	–0.01	1967.8057	–0.02
8	1968.7445	–0.01	1967.6757	–0.17
10	1968.8644	–0.61	1967.5455	0.57
12	1968.9839	–0.51	(1967.4129)[a]	...
14	1969.1029	0.18	1967.2802	0.45
16	1969.2202	0.28	1967.1452	–0.31
18	1969.3361	0.08	1967.0103	0.13
20	1969.4508	–0.22	1966.8737	–0.03
22	1969.5649	–0.02	1966.7361	–0.09
24	1969.6778	0.08	1966.5972	–0.35
26	1969.7896	0.19	1966.4576	–0.20
28	1969.8998	–0.20	1966.3168	–0.15
30	1970.0094	–0.09	1966.1747	–0.30
32	1970.1182	0.33	1966.0321	0.16
34	1970.2254	0.26	1965.8877	–0.08
36	1970.3313	–0.01	1965.7427	0.18
38	1970.4366	0.23	1965.5959	–0.24
40	1970.5405	0.18	1965.4487	0.04
42	1970.6429	–0.26	1965.3004	0.33
44	1970.7448	–0.09	1965.1501	–0.27
46	1970.8452	–0.31	1964.9996	0.05
48	1970.9453	0.28	1964.8481	0.47
50	1971.0432	–0.21	1964.6944	–0.19

[a]Calculated value. No measurement was possible due to idler absorption caused by an atmospheric water line.

than those reported by van Orden, but are still in the range of their estimated errors.

As can be seen from the inset in Fig. 8, there is evidence for a weaker band of transitions, presumably originating from a hot band involving the ν_3 vibrational mode. A detailed analysis of these lines is currently in progress and results will be given elsewhere.

TABLE II. Molecular parameters for the ν_3 fundamental vibration of Si_2C_3 in units of cm^{-1}. The average deviation of the observed to the calculated frequencies is 2.6×10^{-4} cm^{-1}, the experimental uncertainty of the positions in the fit was conservatively set to 5×10^{-4} cm^{-1}, which resulted in a rms value of 0.54.

Parameter	This work	van Orden *et al.* (see Ref. 22)	*Ab initio* (see Ref. 25)
B''	0.0315678(12)	0.0315751(60)	0.0315652
D'' [$\times 10^{-8}$]	<0.08[a]	0.10[b]	...
ν_3	1968.18865(14)	1968.18831(18)	2020[c]
B'	0.0314305(13)	0.0314374(57)	0.0314294[d]
D' [$\times 10^{-8}$]	<0.08[a]	0.10[b]	...

[a]D did not significantly improve the fit. This value has been kept fixed at zero. Given here as an upper limit is the 1σ value of a common D parameter for ground and excited states when released in the fitting procedure.
[b]The authors gave this value as an estimate, believed to be correct within one order of magnitude.
[c]Harmonic value ω_3.
[d]Calculated from vibration-rotation coupling constants given in the reference.

V. CONCLUSION AND OUTLOOK

Using the carbon-silicon cluster Si_2C_3 as a test case, we demonstrated a powerful combination of a cw long-wavelength OPO based on PPLN with a sensitive spectrometer for application in high-resolution spectroscopy of transient molecules. The frequency range of the OPO between 1850 and 2150 cm^{-1} provides superb wavelength coverage in this important spectral region in the MIR. The frequency accuracy achievable with the present setup is of the order of a few MHz. Further improvement of the accuracy may be obtained by stabilizing the OPO signal frequency to a reference interferometer or a frequency comb.[26]

Extension of the OPO coverage towards longer wavelengths is highly desirable and possible, but requires a stronger pump because the threshold will rise drastically because of the increasing absorption coefficient of PPLN towards longer wavelengths. A pump enhanced setup, where the pump power is amplified in a separate resonator would also provide the necessary power levels. Other nonlinear optical materials, such as orientation-patterned GaAs (Ref. 27) would lower the oscillation threshold, but are not yet available commercially.

As mentioned earlier, there are still small frequency gaps where OPO oscillation cannot be reached with our given pump laser due to absorbing water vapor in the OPO cavity. A possibility to overcome this problem is to purge the OPO cavity with dry air or to evacuate it.

Further improvement in sensitivity of the spectrometer may be achieved by using cavity enhanced spectroscopy instead of the multipass reflection cell.

ACKNOWLEDGMENTS

The authors thank I. Breunig, R. Sowade, and J. Kiessling from the University of Bonn for sharing experience and ideas about OPOs. We thank H. Beckers (Bergische Universität Wuppertal, Germany) for the FTIR spectrum of allene. We gratefully acknowledge funding by Deutsche Forschungsgemeinschaft (DFG) (Grant Nos. TH 1301/3-1 and SFB 956) and DFG Grant SFB 494 for initial OPO hardware.

APPENDIX A: FREQUENCY CALIBRATION

For calibration means, the spectrum of a reference gas and fringes of an icFPI are recorded simultaneously to the jet spectrum, using sensitive liquid nitrogen-cooled photovoltaic InSb detectors.

Reference interferometers are commonly used for calibration in frequency scans. Their fringes are assumed to be equidistant in frequency in the process of calibration. Therefore, it is very important that fringes do not change their frequency position during the time of a scan. Commonly used solid germanium etalons are quite sensitive to temperature changes in this respect. An estimation for this temperature sensitivity of the resonance frequency ν of a solid Ge etalon can be made as follows: $\Delta\nu/\nu \approx \Delta n/n = \Delta n/\Delta T \cdot \Delta T/n$ with the refractive index of germanium $n = 4$, the temperature dependence of this

Downloaded 10 Mar 2012 to 134.95.83.67. Redistribution subject to AIP license or copyright; see http://rsi.aip.org/about/rights_and_permissions

coefficient[28] $\Delta n/\Delta T = 4 \times 10^{-4}$. Here, the length expansion of germanium can be neglected, because the linear expansion coefficient is roughly two orders of magnitude lower. A small temperature variation of $\Delta T = 10^{-2}$ K then results in a drift of the resonance frequency of the Ge etalon of 2×10^{-3} cm^{-1} at a frequency of 2000 cm^{-1}. When using such an etalon, one has to make sure that its temperature is very stable during measurement, which can take an hour and more in our case.

The icFPI we use in the experiment is designed to be insensitive to temperature changes and as such avoids the problems depicted. The setup and properties of our icFPI are described in Ref. 29. The icFPI is evacuated and therefore has negligible coefficients for $\Delta n/\Delta T$, and the thermal expansion of the spacings between the interferometer mirrors is also compensated in the construction. This makes the icFPI an ideal tool for calibrating spectra.

Allene, C_3H_4, has been used as a reference gas. It exhibits a strong and dense spectrum around 5 μm, making it well suited for the calibration purposes described here. An allene spectrum covering the range around 1950 cm^{-1} was recorded using the Fourier transform infrared spectrometer at Bergische Universität Wuppertal.

Final frequency calibration was executed by flattening the spectrum so that etalon fringes were equidistant in the data. After that, the frequency information of the scan was altered using a linear function, so that the observed reference gas spectrum coincided with the known frequency positions. In overlapping scans, positions of observed target molecule transitions were also taken into account. In the present study, fitting of the desired linear functions was done manually. The accuracy reached here is approximately of 5×10^{-4} cm^{-1} ($\approx$ 15 MHz).

APPENDIX B: OPO-THEORY WITH ABSORPTION

Equations (2)–(4) are greatly simplified to two coupled equations, assuming a constant pump field $\mathcal{E}_p(z) = \mathcal{E}_p$. This approximation holds when the conversion efficiency is low and the pump absorption is negligible:

$$\frac{\partial}{\partial z}\mathcal{E}_s(z) = i\gamma_s\,\mathcal{E}_p\mathcal{E}_i^*(z)\,e^{+i\Delta k z} - \frac{\alpha_s}{2}\mathcal{E}_s(z), \qquad \text{(B1)}$$

$$\frac{\partial}{\partial z}\mathcal{E}_i(z) = i\gamma_i\,\mathcal{E}_p\mathcal{E}_s^*(z)\,e^{+i\Delta k z} - \frac{\alpha_i}{2}\mathcal{E}_i(z). \qquad \text{(B2)}$$

With the *ansatz* $\mathcal{E}_l(z) = \tilde{\mathcal{E}}_l e^{(\Gamma + i(\Delta k/2))z}$ $(l = s, i)$, where $\tilde{\mathcal{E}}_l$ are constant amplitudes independent of z, we find a characteristic equation for Γ:

$$\left[\left(\Gamma + i\frac{\Delta k}{2} + \frac{\alpha_s}{2}\right)\left(\Gamma - i\frac{\Delta k}{2} + \frac{\alpha_i}{2}\right) - \gamma_s\gamma_i|\mathcal{E}_p|^2\right]\tilde{\mathcal{E}}_s = 0.$$

For the non-trivial case $\tilde{\mathcal{E}}_s \neq 0$, the term in the square brackets vanishes, which results in a quadratic equation for Γ with two independent results $\Gamma_\pm$:

$$\Gamma_\pm = -\underbrace{\frac{1}{4}(\alpha_i + \alpha_s)}_{=\alpha} \pm \underbrace{\sqrt{\delta^2 + \gamma_s\gamma_i|\mathcal{E}_p|^2}}_{=g}$$

using the abbreviation $\delta = (\alpha_i - \alpha_s - 2i\Delta k)/4$. Now the coupled wave equations take the form

$$\mathcal{E}_s(z) = \left(\tilde{\mathcal{E}}_s^+ e^{+gz} + \tilde{\mathcal{E}}_s^- e^{-gz}\right) e^{-\alpha z} e^{(i\Delta k 2)z},$$
$$\mathcal{E}_i(z) = \left(\tilde{\mathcal{E}}_i^+ e^{+gz} + \tilde{\mathcal{E}}_i^- e^{-gz}\right) e^{-\alpha z} e^{i(\Delta k/2)z}$$

with the parameters $\alpha = (\alpha_s + \alpha_i)/4$ as a mean value for signal and idler absorption coefficients and $g^2 = \gamma_s\gamma_i|\mathcal{E}_p|^2 + \delta^2 = g_\star^2 + \delta^2$ as a driving term, including pump intensity, nonlinear coupling factors, and also absorption coefficients as well as phase mismatch. The amplitude coefficients $\tilde{\mathcal{E}}_{s,i}^\pm$ have to be determined by the boundary conditions. In a singly resonant OPO, like in the present case, there is no idler wave incident at the front facet of the nonlinear crystal, which gives $\mathcal{E}_i(0) = \mathcal{E}_i^*(0) = 0$, while the signal wave amplitude is non-zero: $\mathcal{E}_s(0) = \mathcal{E}_{s0}$. These two conditions lead to $\tilde{\mathcal{E}}_s^- = \mathcal{E}_{s0} - \tilde{\mathcal{E}}_s^+$ and $\tilde{\mathcal{E}}_i^- = -\tilde{\mathcal{E}}_i^+$; thus, the solutions can be expressed using the hyperbolic sine function:

$$\mathcal{E}_s(z) = 2\tilde{\mathcal{E}}_s^+ \sinh(gz)\,e^{i(\Delta k/2)z}e^{-\alpha z} \quad + \mathcal{E}_{s0}e^{-gz}e^{i(\Delta k/2)z}e^{-\alpha z},$$
$$\mathcal{E}_i(z) = 2\tilde{\mathcal{E}}_i^+ \sinh(gz)\,e^{i(\Delta k/2)z}e^{-\alpha z}.$$

By calculating $(\partial/\partial z)\mathcal{E}_s(z)\big|_{z=0}$ and $(\partial/\partial z)\mathcal{E}_i(z)\big|_{z=0}$ and comparing to the right sides of Eqs. (B1) and (B2) at position $z = 0$, one obtains for the amplitude coefficients,

$$\tilde{\mathcal{E}}_s^\pm = \frac{1}{2}\left(1 \pm \frac{\delta}{g}\right)\mathcal{E}_{s0},$$
$$\tilde{\mathcal{E}}_i^\pm = \pm i\frac{\gamma_i}{2g}\mathcal{E}_p\mathcal{E}_{s0}^*.$$

The gain the signal wave experiences upon a single pass through the nonlinear medium of length l is called G_s and can be expressed as

$$G_s = \frac{I_s(l) - I_s(0)}{I_s(0)} = \frac{I_s(l)}{I_s(0)} - 1 = \frac{|\mathcal{E}_s(l)|^2}{|\mathcal{E}_s(0)|^2} - 1.$$

Substituting the above found solutions results in the expression,

$$G_s = \left|\cosh(gl) + \frac{\delta}{g}\sinh(gl)\right|^2 e^{-2\alpha z} - 1.$$

Neglecting absorption $(\alpha_i = \alpha_s = 0)$ and assuming perfect phase matching $(\Delta k = 0)$, the parameter δ equals zero and the above equation reduces to the simple expression $G_s = \sinh^2(g_\star l) \approx g_\star^2 l^2$ with $g_\star$ as the factor of g, when no absorption or phase mismatch is present: $g_\star = (2\omega_s\omega_i d^2 I_p)/(\varepsilon_0 n_p n_s n_i c^3)$.

The threshold can now be calculated by assuming that the signal intensity at the front facet of the crystal is reproduced after being amplified in the crystal and attenuated by losses V during one cavity round trip. This results in

$$G_s(\mathcal{E}_{p,\mathrm{th}}) = \frac{V}{1 - V}.$$

By substituting the signal gain found above, the threshold pump power can be deduced.

[1]P. Neubauer-Guenther, T. F. Giesen, U. Berndt, G. Fuchs, and G. Winnewisser, Spectrochim. Acta, Part A **59**, 431 (2003).

Downloaded 10 Mar 2012 to 134.95.83.67. Redistribution subject to AIP license or copyright; see http://rsi.aip.org/about/rights_and_permissions

[2]J. Krieg, V. Lutter, F. Hardy, S. Schlemmer, and T. Giesen, J. Chem. Phys. **132**, 224306 (2010).
[3]G. Sonnabend, D. Wirtz, and R. Schieder, Appl. Opt. **44**, 7170 (2005).
[4]J. Armstrong, N. Bloembergen, J. Ducuing, and P. Pershan, Phys. Rev. **127**, 1918 (1962).
[5]L. Myers, R. Eckardt, M. Fejer, R. Byer, W. Bosenberg, and J. Pierce, J. Opt. Soc. Am. B **12**, 2102 (1995).
[6]S. Yang, R. Eckardt, and R. Byer, Opt. Lett. **18**, 971 (1993).
[7]A. Ngai, S. Persijn, G. von Basum, and F. Harren, Appl. Phys. B: Lasers Opt. **85**, 173 (2006).
[8]M. Vainio, J. Peltola, S. Persijn, F. Harren, and L. Halonen, Opt. Express **16**, 11141 (2008).
[9]L. E. Myers, R. C. Eckardt, M. M. Fejer, R. L. Byer, and W. R. Bosenberg, Opt. Lett. **21**, 591 (1996).
[10]G. Turnbull, D. McGloin, I. Lindsay, M. Ebrahimzadeh, and M. Dunn, Opt. Lett. **25**, 341 (2001).
[11]J. Kiessling, R. Sowade, I. Breunig, K. Buse, and V. Dierolf, Opt. Express **17**, 87 (2009).
[12]W. Bosenberg, A. Drobshoff, J. Alexander, L. Myers, and R. Byer, Opt. Lett. **21**, 1336 (1996).
[13]S. Persijn, F. Harren, and A. van der Veen, Appl. Phys. B: Lasers Opt. **100**, 383 (2010).
[14]See www.innolight.de for Innolight GmbH, Garbsener Landstr. 10, 30419 Hannover, Germany.
[15]See www.layertec.de for Layertec GmbH, Ernst-Abbe-Weg 1, 99441 Mellingen, Germany.
[16]L. Rothman, D. Jacquemart, A. Barbe, D. Chris Benner, M. Birk, L. Brown, M. Carleer, C. Chackerian, *et al.* J. Quant. Spectrosc. Radiat. Transf. **96**, 139 (2005)
[17]O. Gayer, Z. Sacks, E. Galun, and A. Arie, Appl. Phys. B: Lasers Opt. **91**, 343 (2008).
[18]R. L. Byer and R. L. Herbst, in *Topics in Applied Physics: Nonlinear Infrared Generation*, edited by Y. R. Shen (Springer, Berlin, 1977), Vol. 16, pp. 87–137.
[19]D. Lowenthal, IEEE J. Quantum Electron. **34**, 1356 (1998).
[20]See www.lohnstaroptics.com for LohnStar Optics Inc., 1863 Commercial St., Escondido, 92029, USA.
[21]A. van Orden and R. Saykally, Chem. Rev. **98**, 2313 (1998).
[22]A. van Orden, T. F. Giesen, R. A. Provencal, H. J. Hwang, and R. J. Saykally, J. Chem. Phys. **101**, 10237 (1994).
[23]C. M. Western, PGOPHER, a Program for Simulating Rotational Structure, version 7.1, University of Bristol; also see http://pgopher.chm.bris.ac.uk.
[24]H. M. Pickett, J. Mol. Spectrosc. **148**, 371 (1991).
[25]P. Botschwina, J. Mol. Spectrosc. **198**, 192 (1999).
[26]H. Inaba, T. Ikegami, F. L. Hong, A. Onae, Y. Koga, T. R. Schibli, K. Minoshima, H. Matsumoto, S. Yamadori, O. Tohyama, and S. I. Yamaguchi, IEEE J. Quantum Electron. **40**, 929 (2004)
[27]L. Eyres, P. Tourreau, T. Pinguet, C. Ebert, J. Harris, M. Fejer, L. Becouarn, B. Gerard, and E. Lallier, Appl. Phys. Lett. **79**, 904 (2001).
[28]H. Icenogle, B. Platt, and W. Wolfe, Appl. Opt. **15**, 2348 (1976).
[29]M. Reich, R. Schieder, H. J. Clar, and G. Winnewisser, Appl. Opt. **25**, 130 (1986).

Downloaded 10 Mar 2012 to 134.95.83.67. Redistribution subject to AIP license or copyright; see http://rsi.aip.org/about/rights_and_permissions